Fluidic microoptics with adjustable focusing and beam steering for single cell optogenetics

As Published: 10.1364/OE.25.016825

Publisher: The Optical Society

Persistent URL: https://hdl.handle.net/1721.1/135742

Version: Final published version: final published article, as it appeared in a journal, conference proceedings, or other formally published context

Research Article | Vol. 25, No. 14 | 10 Jul 2017 | OPTICS EXPRESS 16825
Optics EXPRESS

Fluidic microoptics with adjustable focusing and beam steering for single cell optogenetics

SHAUN BERRY,[1,*] SHAWN REDMOND,[1] PAUL ROBINSON,[1] TODD THORSEN,[1] MORDECHAI ROTHSCHILD,[1] AND EDWARD S. BOYDEN[2]

[1]*MIT Lincoln Laboratory, 244 Wood St., Lexington, MA 02421, USA*
[2]*Departments of Biological Engineering and Brain and Cognitive Sciences, Media Lab and McGovern Institute, MIT, 43 Vassar St., Cambridge, MA 02139, USA*
**sberry@LL.mit.edu*

Abstract: Electrically controlled micron-scale liquid lenses have been designed, fabricated and demonstrated, that provide both adjustable focusing and beam steering, with the goal of applying them to optogenetic *in vivo* mapping of brain activity with single cell resolution. The liquid lens is formed by the interface between two immiscible liquids which are contained in a conically tapered lens cavity etched into a fused silica substrate. Interdigitated electrodes have been patterned along the sidewall of the taper to control the liquid lens curvature and tilt. Microlenses with apertures ranging in size from 30 to 80 μm were fabricated and tunable focusing ranging from 0.25 to 3 mm and beam steering of ± 1 degree have been demonstrated.

OCIS codes: (220.0220) Optical design and fabrication; (220.3630) Lenses.

References and links

1. K. Deisseroth, G. Feng, A. K. Majewska, G. Miesenböck, A. Ting, and M. J. Schnitzer, "Next-generation optical technologies for illuminating genetically targeted brain circuits," J. Neurosci. **26**(41), 10380–10386 (2006).
2. E. S. Boyden, F. Zhang, E. Bamberg, G. Nagel, and K. Deisseroth, "Millisecond-timescale, genetically targeted optical control of neural activity," Nat. Neurosci. **8**(9), 1263–1268 (2005).
3. N. C. Klapoetke, Y. Murata, S. S. Kim, S. R. Pulver, A. Birdsey-Benson, Y. K. Cho, T. K. Morimoto, A. S. Chuong, E. J. Carpenter, Z. Tian, J. Wang, Y. Xie, Z. Yan, Y. Zhang, B. Y. Chow, B. Surek, M. Melkonian, V. Jayaraman, M. Constantine-Paton, G. K. Wong, and E. S. Boyden, "Independent optical excitation of distinct neural populations," Nat. Methods **11**(3), 338–346 (2014).
4. J. P. Rickgauer and D. W. Tank, "Two-photon excitation of channelrhodopsin-2 at saturation," Proc. Natl. Acad. Sci. U.S.A. **106**(35), 15025–15030 (2009).
5. B. K. Andrasfalvy, B. V. Zemelman, J. Tang, and A. Vaziri, "Two-photon single-cell optogenetic control of neuronal activity by sculpted light," Proc. Natl. Acad. Sci. U.S.A. **107**(26), 11981–11986 (2010).
6. E. Papagiakoumou, F. Anselmi, A. Bègue, V. de Sars, J. Glückstad, E. Y. Isacoff, and V. Emiliani, "Scanless two-photon excitation of channelrhodopsin-2," Nat. Methods **7**(10), 848–854 (2010).
7. Y. Fainman, D. Psaltis, and C. Yang, *Optofluidics: Fundamentals, Devices, and Applications* (McGraw Hill, 2010).
8. D. Psaltis, S. R. Quake, and C. Yang, "Developing optofluidic technology through the fusion of microfluidics and optics," Nature **442**(7101), 381–386 (2006).
9. L. Pang, H. M. Chen, L. M. Freeman, and Y. Fainman, "Optofluidic devices and applications in photonics, sensing and imaging," Lab Chip **12**(19), 3543–3551 (2012).
10. N. Chronis, G. Liu, K. H. Jeong, and L. Lee, "Tunable liquid-filled microlens array integrated with microfluidic network," Opt. Express **11**(19), 2370–2378 (2003).
11. M. Agarwal, R. A. Gunasekaran, P. Coane, and K. Varahramyan, "Polymer-based variable focal length microlens system," J. Micromech. Microeng. **14**(12), 1665–1673 (2004).
12. W. Wang and J. Fang, "Variable focusing microlens chip for potential sensing applications," IEEE Sens. J. **7**(1), 11–18 (2007).
13. C. A. Lopez, C. C. Lee, and A. H. Hirsa, "Electrochemically activated adaptive liquid lens," Appl. Phys. Lett. **87**(13), 134102 (2004).
14. S. Xu, H. Ren, and S. T. Wu, "Dielectrically tunable optofluidic devices," J. Phys. D Appl. Phys. **46**(48), 483001 (2013).
15. S. Kupier and B. H. W. Hendriks, "Variable-focus liquid lens for miniature cameras," Appl. Phys. Lett. **85**(7), 1128–1130 (2004).
16. B. Berge and J. Peseux, "Variable focus lens controlled by an external voltage: An application of electrowetting," Eur. Phys. J. E **3**(2), 159–163 (2000).

#295262 https://doi.org/10.1364/OE.25.016825
Journal © 2017 Received 4 May 2017; revised 30 Jun 2017; accepted 5 Jul 2017; published 7 Jul 2017

Optics EXPRESS

17. F. Mugele and J. Baret, "Electrowetting: from basics to applications," J. Phys. Condens. Matter **17**(28), R705–R774 (2005).
18. D. Kopp and H. Zappe, "Tubular astigmatism-tunable fluidic lens," Opt. Lett. **41**(12), 2735–2738 (2016).
19. D. Kopp, T. Brender, and H. Zappe, "All-liquid dual-lens optofluidic zoom system," Appl. Opt. **56**(13), 3758–3763 (2017).
20. A. M. Watson, K. Dease, S. Terrab, C. Roath, J. T. Gopinath, and V. M. Bright, "Focus-tunable low-power electrowetting lenses with thin Parylene films," Appl. Opt. **54**(20), 6224–6229 (2015).
21. N. R. Smith, D. C. Abeysinghe, J. W. Haus, and J. Heikenfeld, "Agile wide-angle beam steering with electrowetting microprisms," Opt. Express **14**(14), 6557–6563 (2006).
22. C. E. Clement and S. Y. Park, "High-performance beam steering using electrowetting-driven liquid prism fabricated by a simple dip-coating method," Appl. Phys. Lett. **108**(19), 191601 (2016).
23. C. U. Murande, J. M. Oh, D. van de Ende, and F. Mugele, "Electrowetting driven optical switch and tunable aperture," Opt. Express **19**(16), 15526–15531 (2011).
24. K. Zhou, J. Heikenfeld, K. A. Dean, E. M. Howard, and M. R. Johnson, "A full description of a simple and scalable fabrication process for electrowetting displays," JMEMS **19**, 065029 (2009).
25. A. N. Zorzos, J. Scholvin, E. S. Boyden, and C. G. Fonstad, "Three-dimensional multiwaveguide probe array for light delivery to distributed brain circuits," Opt. Lett. **37**(23), 4841–4843 (2012).
26. E. Simon, B. Berge, F. Fillit, H. Gaton, M. Guillet, O. Jacques-Sermet, F. Laune, J. Legrand, M. Maillard, and N. Tallaron, "Optical design rules of a camera module with a liquid lens and principle of command for AF and OIS functions," in *Proceedings of Optical Design and Testing IV*, Y. Wang, *et al.* ed. (SPIE 2010), 784903.
27. S. R. Berry, J. B. Stewart, T. A. Thorsen, and I. Guha, "Development of adaptive liquid microlenses and microlens arrays," in *Proceedings of MOEMS and Miniaturized Systems XII*, W. Piyawattanametha, and Y. H. Park, ed. (SPIE 2013), 861610.
28. M. Sussman, P. Smereka, and S. Osher, "A level set approach for computing solutions to incompressible two-phase flow," J. Comput. Phys. **114**(1), 146–159 (1994).
29. M. Maillard, J. Legrand, and B. Berge, "Two liquids wetting and low hysteresis electrowetting on dielectric applications," Langmuir **25**(11), 6162–6167 (2009).
30. S. Berry, J. Kedzierski, and B. Abedian, "Irreversible electrowetting on thin fluoropolymer films," Langmuir **23**(24), 12429–12435 (2007).
31. C. M. Waits, B. Morgan, M. Kastantin, and R. Ghodssi, "Microfabrication of 3D silicon MEMS structures using gray-scale lithography and deep reactive ion etching," Sens. Actuators A Phys. **119**(1), 245–253 (2005).
32. M. Fritze, J. Knecht, C. Bozler, C. Keast, J. Fijol, S. Jacobson, P. Keating, J. LeBlanc, E. Fike, B. Kessler, M. Frish, and C. Manolatou, "Fabrication of three-dimensional mode converters for silicon-based integrated optics," J. Vac. Sci. Technol. B **21**(6), 2897–2902 (2003).
33. A. E. Siegman, *Lasers* (University Science Books, 1986), Chap. 20.
34. F. Li and F. Mugele, "How to make sticky surfaces slippery: Contact angle hysteresis in electrowetting with alternating voltage," Appl. Phys. Lett. **92**(24), 244108 (2008).
35. C. U. Murade, D. van der Ende, and F. Mugele, "High speed adaptive liquid microlens array," Opt. Express **20**(16), 18180–18187 (2012).

1. Introduction

In the last decade, optogenetics has emerged as a powerful tool to monitor and control the functioning of populations of neurons *in vivo* [1]. Optogenetics consists of the selective photoexcitation of neurons, genetically modified to express photosensitive membrane proteins (opsins) [2]. Upon excitation, these opsins react by transporting ions into or out of neurons to control their electrical activity. So far, most optogenetics studies have involved photoexcitation with limited spatial resolution, relying on orthogonal genetically-modified channelrhodopsins that respond to different colors of light that are selectively expressed in different classes of neurons [3]. Two-photon control is possible, but only within the shallow depths (e.g. <1 mm) afforded by two-photon penetration into the brain [4–6]. Thus, it is highly desirable to have a method of exciting individual neurons at arbitrary sites in the brain in a controllable and single-cell manner, as this would open the possibility of *in vivo* analysis of network connectivity at the single-cell level, even in difficult-to-access deep brain tissue. Our ultimate goal is to develop an implantable optical probe that has active focusing and steering optics placed at the end of the probe that will enable light delivery from an external laser to individual neurons.

To minimize cell damage during insertion, the optical probe with the integrated optics needs to be as small as possible, ideally <300 μm for both the width and thickness dimensions. This means the optics for active focusing and beam steering have to be on the order of 10's of microns. At this size scale, mechanical lens systems would be too large for

Optics EXPRESS

this application. Fortunately, there has been substantial research into tunable micro-optofluidic devices [7–9], including optofluidic lenses. Optofluidic lenses formed from fluids are an attractive approach since they scale well to small dimensions. At these length scales, surface tension will dominate the interface shape which is either a liquid-air or liquid-liquid interface, producing a smooth spherical lens profile. In addition, the lenses can be adaptively tuned by pneumatic actuation [10,11], thermal actuation [12], electrochemistry [13], dielectrophoresis [14], and electrowetting [15,16].

In particular, electrowetting, described in detail elsewhere [17], is an attractive way to control liquid interfaces because it requires no moving parts, is a reversible process, and consumes very low power, which is important in this application since no heat can be generated by the lensing system because it can affect neuron activity. In electrowetting, the surface energy of the solid substrate is modified by the application of a voltage, changing it from hydrophobic to hydrophilic in prescribed regions via suitably designed electrodes covered by a hydrophobic dielectric film. There has been considerable research into electrowetting-based; tunable optofluidic lenses [15, 16, 18–20]. Electrowetting liquid lenses have even been commercialized by Varioptic (now part of Invenios). In addition to active focusing elements, other electrowetting adaptive optics devices have been demonstrated, such as beam steers [21,22], irises [23] and displays [24].

Here we discuss progress that we have made in the first phase of our work, namely engineering micron-scale liquid lenses using electrowetting to control the curvature and shape of the liquid interface to enable both focusing and steering combined in a single optical element. This is achieved by a novel design of the substrate consisting of a conical taper, which contains the two immiscible liquids. These liquid lenses are designed so that in later phases of the program they can be fabricated monolithically to waveguides operating in the red/near-infrared. This work builds from previous work we have done on microfabricated waveguide-mediated optogenetic control [25], thus enabling two-photon optogenetic excitation of individual cells at arbitrary locations in living mammalian brains.

2. Design, fabrication, and packaging

2.1 Design

A target volume containing ~100,000 neuron cell bodies requires a microlens system to have a focus range of 0.1 – 1 mm with simultaneous steering over ± 5°. In addition, to be useful for stimulating neural activity the microlens must focus the light down to a spot size of ~10 μm, roughly the size of a neuron cell body. To minimize the overall size of the optic, both focusing and steering adjustments are made via a single optical element. Both functionalities are achieved by embedding the liquid interface in a conical taper, etched into a fused silica substrate, as shown in Fig. 1, which has interdigitated electrodes along the sidewall that are covered with two dielectric layers, a silicon dioxide film and a hydrophobic film. Initial designs employ four independent electrodes or a single electrode around the conical taper.

In electrowetting, one of the liquids needs to be conductive, typically water, and the other phase, an insulator, typically a non-polar solvent like oil. The positioning of the oil and water forms the microlens and is controlled by a patterned hydrophobic film over the electrodes and a surrounding hydrophilic surface. In this design, oil resides inside the taper over the patterned hydrophobic film. When a voltage is applied the surface energy changes from hydrophobic to more hydrophilic, allowing water to wet over the electrode, thus changing the radius of curvature. Since the index of refraction for oils, n_o, is typically greater than the index of refraction of water, n_w, variable focusing can be achieved. The liquid lens focuses along the optical axis when the same voltage is applied to all the electrodes. This results in the contact line at the liquid-liquid-solid interface to move uniformly along the taper side wall as a function of voltage, Fig. 1(b).

Optics EXPRESS

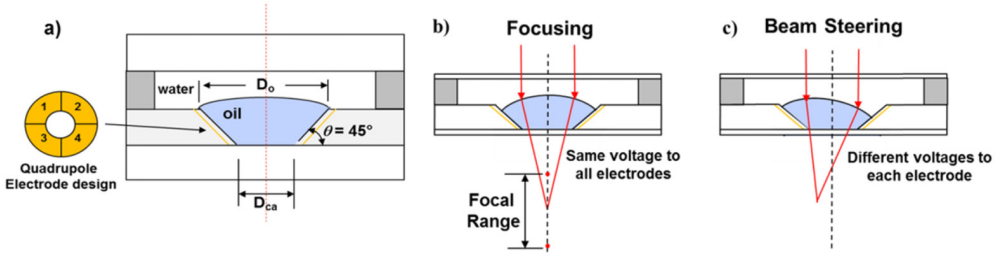

Fig. 1. a) Liquid microlens design that combines both active focusing and steering by controlling the interface formed between two immiscible liquids. D_o is the lens diameter and D_{ca} is the clear aperture diameter. The liquid interface is contained within a 45° conical taper that has a series of patterned metal electrodes along the sidewall. b) Variable focusing along the optical path will occur when the same potential is applied to all the electrodes. c) Beam steering will occur when different potentials are applied to each electrode pair.

To effectively focus and steer the light simultaneously, the liquid interface needs to piston, i.e. tilt. This is accomplished as a result of the tapered geometry and applying different voltages to different electrode pairs, Fig. 1(c). It should be noted that Varioptic has commercialized a similar design used for image stabilization that consists of a machined conical taper profile having interdigitated electrodes patterned around the annulus [26]. Currently, the Varioptic lenses are on the size of millimeters, which are too large for this application. In this work the liquid lenses being developed are an order of 10's of microns. In this phase of the project four different microlens cavity sizes were fabricated, nominally with an outside diameter, D_o, of 50 µm, 60 µm, 75 µm and 100 µm. These size microlenses where chosen since the estimated focal lengths, based on our previous work with planar liquid microlenses [27] and the typical values of the index of refraction for the water and oil phases, would be within the design criteria of $f = 0.1$ to 1 mm.

To determine the appropriate taper angle and taper depth, numerical simulations were used to help guide the microlens cavity design. Two-dimensional, two-phase numerical simulations, using the level-set method [28] were used to track the liquid interface in the taper cavity. Equivalent analytical models could have also been derived, however using numerical simulations allowed for rapid assessment and visualization of different geometry configurations. The numerical simulations were performed using the commercially available software package, COMSOL Multiphysics® v5.2. In the model, a no-slip wall boundary condition was used for all the exterior walls except for the two walls forming the conical taper. The boundary condition was set as a wetted-wall for these walls, where the contact angle is defined. Instead of modeling the full electromechanical problem, a voltage-dependent contact angle was defined using the Lippmann-Young equation [29] for an oil drop surrounded by water ambient:

$$\theta(V) = \cos^{-1}\left[\cos\left(\theta^o\right) - \frac{CV^2}{2\gamma_{wo}}\right] \tag{1}$$

where θ^o is Young's angle, C is the capacitance of the dielectric stack, which for this work consisted of two films, a 500-nm thick silicon dioxide film and a 85-nm thick hydrophobic film (discussed in Section 2.2), V is the applied voltage, and γ_{wo} is the surface tension between the water and oil phase.

In the simulations, voltages from zero to a V_{max} were applied and the equilibrium interface shape solved for each new contact angle. V_{max} was set to the voltage value that would just initiate dielectric breakdown of the hydrophobic film, which for this film thickness and material, CYTOP 809M, was estimated to be 40 V. This design criterion comes from a prior study [30] where poor electrowetting behavior is experienced when dielectric breakdown occurs in the hydrophobic film. Figure 2 shows simulation results from several different

Optics EXPRESS

microlens cavity designs with different taper angles having a clear aperture of 32 µm and a cavity depth of 15 µm. The liquid properties used in the simulations were for deionized water and dodecane (oil phase), where $\theta° = 23°$, and $\gamma_{wo} = 45$ mN/m.

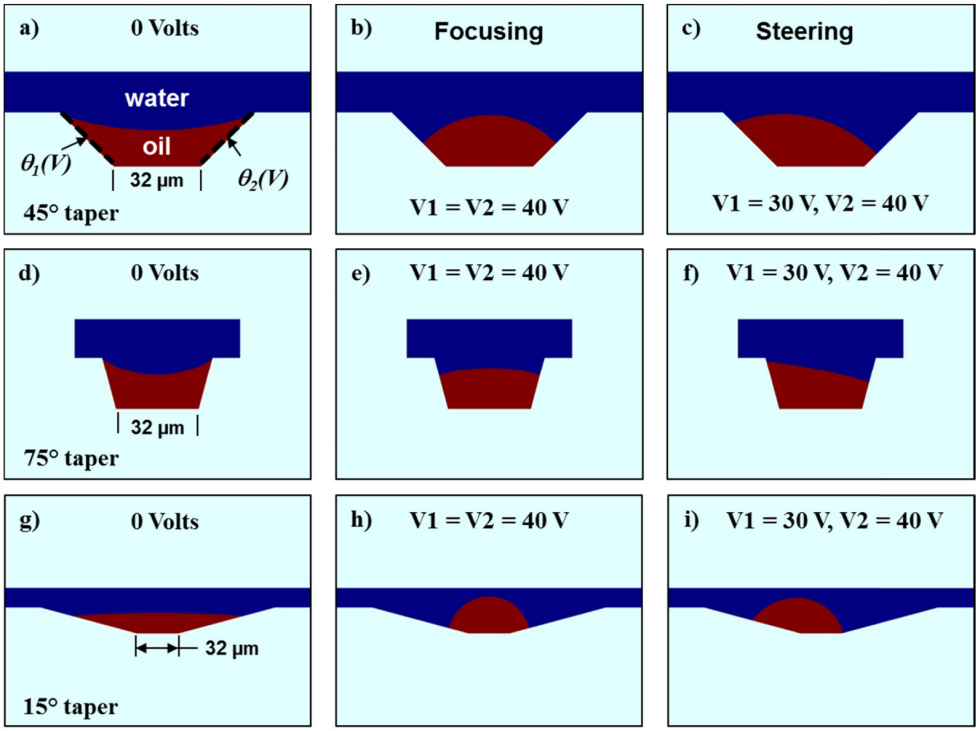

Fig. 2. Numerical simulation results for microlens cavities having different taper angles. The liquid properties in the simulations were for deionized water and dodecane (oil phase), where $\theta° = 23°$, and $\gamma_{wo} = 45$ mN/m. The clear aperture was set at 32 µm and the cavity depth was 15 µm. a) Interface profile at 0 V for 45° taper. b) Focusing condition when $V1 = V2$ for 45° taper. c) Beam steering $V1 < V2$ for 45° taper. d) Interface profile at 0 V for 75° taper. e) Focusing condition when $V1 = V2$ for 75° taper. f) Beam steering $V1 < V2$ for 75° taper. g) Interface profile at 0 V for 15° taper. h) Focusing condition when $V1 = V2$ for 15° taper. i) Beam steering $V1 < V2$ for 15° taper.

The results show that as the taper angle increases, the initial interface shape at 0 V becomes more concave, Figs. 2(a), 2(d), 2(g), since the equilibrium contact angle on the taper side wall is becoming larger relative to the increases in taper angle. A concave interface shape means the liquid microlens will have a negative optical power. This also means larger voltages need to be applied to change the interface shape to convex in order for the liquid microlens to have positive optical power for large taper angles. The interface curvature changes from concave to convex at ~36 V for the 75° taper design compared to only ~14 V for the 45° taper design. This results in a greater operating range before the dielectric breakdown voltage is reached for the 45° taper design. In the case for shallow taper angles less than Young's angle, $\theta°$, the liquid microlens curvature will be convex at 0 V and have positive optical power. However, there are several issues associated with a shallow taper angle. First, for nearly any voltage difference applied to the electrodes when the same thickness dielectric is used, the liquid interface that experiences the greater voltage always translates to the bottom of the taper as seen in Fig. 2(i). This will limit the potential achievable steering angles since intermediate interface positions along the side wall will be hard to control. This behavior is not seen as the taper angle increases. In addition, the more plane the substrate becomes, the greater the liquid microlens asymmetry for the multiple

Optics EXPRESS

electrode designs when different voltages are applied. Although not captured in these 2D simulations, our own work with planar liquid lenses having quadrupole electrode designs did reveal considerable lens asymmetry and thus the need for a tapered liquid microlens cavity.

Conversely, as the taper angle increases to 90°, the liquid interface flattens and becomes more like a prism, Fig. 2(f) when different voltages are applied. This behavior would be ideal if beam steering was the main goal since large steering angles can be achieved [21, 22]. However for this application the optic not only has to beam steer but also focus, thus the interface must still maintain a spherical shape even when it tilts inside the cavity. Figure 2(c) shows the liquid interface for a 45° taper that still has a curved shape and thus would not only beam steer but focus as well. Focusing and steering results will be presented in Section 3. Based on the simulation results, a microlens cavity design with a taper angle of 45° and a depth of 15 µm was chosen to be fabricated for this initial phase of the project.

2.2 Fabrication

To form the conical taper in a fused silica substrate, a grayscale-lithography technique was used [31, 32]. Grayscale-lithography allows for 3-D structures to be created using planar microfabrication processes. In this technique, a photolithography mask is created that has feature sizes smaller than the resolution size of the optical exposure system. The sub-resolution features modulate the intensity of ultraviolet light which will expose the photoresist to specified depths. This results in a gradient profile in the resist height after being developed. The photoresist profile can then be transferred into a substrate during an etch process.

The photolithography tool used in this work was a Canon i-line stepper (FPA-3000) that has a 50-mm field size, and an exposure wavelength of λ = 365 nm. Based on the optical parameters of the tool, the resolution limit is 895 nm in wafer units. To form the conical taper, the photomask was designed with sub-resolution annular lines with radially varying line widths. A constant pitch of 895 nm was used and the line widths varied from the smallest size at the inner radius of the taper design to allow for more light exposure and the most penetration into a positive resist, to the widest line widths at the outer radius. Several test masks were designed in order to determine the proper range of line widths and distribution pattern. For the final mask used to form the conical tapered tested in this work, a linear line width distribution from 340 nm to 550 nm was found to produce the desired taper angle in the photoresist.

The taper profiles were formed in 5-µm thick binary photoresist (Shipley SPR220) using an exposure energy of 4900 J/m^2. After the resist was developed, the wafer was placed in 150°C oven for 5 min to reflow the resist. This reflow process smoothed the resist profile, especially near the transitions at the inner and outer taper diameters, Fig. 3(a). The tapered pattern was then transferred into the fused silica using an optimized reactive ion etch (RIE) process. The optimized etch process created a 12-µm deep conical taper with a 45° sloping sidewall, Fig. 3(b). Next, 200-nm of sputtered aluminum was used to form the electrodes. Some microlenses had a quadrupole electrode arrangement and for others only a single circular electrode was used. In order to pattern the electrodes, a spray coating process was used to apply the resist. A 3-µm thick resist (MicroChemicals AZ 9260 diluted with PGMA and acetone 1:1:8) was spray coated over the wafer at 1-µm thick film steps to form a conformal coating. Because the conical taper was 12-µm deep, and a 2-µm gap between electrodes was needed to be maintained for the quadrupole designs, a focus depth of –4.0 µm and high exposure dose of 9500 J/m^2 for the lithography system were found to produce the best results in the resist pattern, especially at the bottom of the taper. Once the resist was patterned, a chlorine-gas-based dry etch process was used to form the electrodes along the taper side wall, Figs. 3(c) and 3(d). After the electrodes were formed, 500 nm of PECVD silicon dioxide was deposited, forming a dielectric layer.

Optics EXPRESS

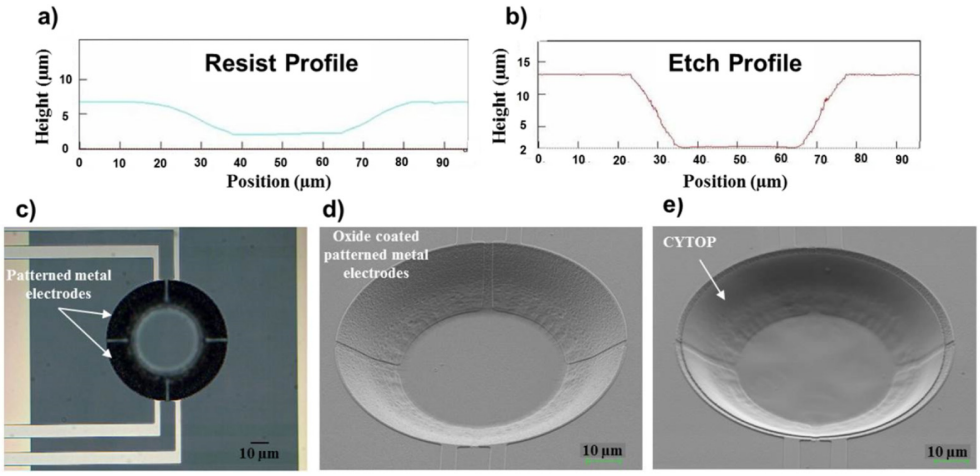

Fig. 3. a) Measured resist profile after reflow at 150°C, for a 50 µm outside diameter and 28 µm clear aperture lens design. Image captured from a 3-D microscope (Keyence). b) Measured etch profile in fused silica. Final lens cavity dimensions: 55 µm outside diameter, 32 µm clear aperture, 12 µm etch depth, and 43° taper angle. Image captured from a 3-D microscope. c) Top-down microscope image of quadrupole electrode design after metal patterning and etch. d) SEM image of quadrupole electrode design after depositing 500 nm of PECVD oxide. e) SEM image after CYTOP processing.

The final fabrication process was to create the hydrophobic/hydrophilic regions. In order for the microlens to function properly, the taper sidewalls need to be hydrophobic. 3% by weight of the amorphous fluoropolymer CYTOP 809M (Asahi Glass) was spun over the wafer at 1000 RPM for 10 sec, and then baked at 150°C for 10 min. This process created an 85-nm thick conformal film. Since the entire wafer surface is now hydrophobic, finding a photoresist that will adhere to the surface was difficult. We found that adding 4% of the fluorocarbon surfactant, FC-4430 to SPR518 resist resulted in the resist spinning perfectly and adhering to the CYTOP film. The CYTOP film was then patterned and etched in oxygen plasma to form hydrophobic regions inside the taper over the electrodes, leaving hydrophilic regions elsewhere Fig. 3(e).

2.3 Packaging

After wafer-scale fabrication, the wafer was diced into 10 mm x 10 mm die (test chip), where each test chip contains 44 microlens cavities. The ultimate goal is to package and integrate only a single liquid lens to an optical probe. However for an initial demonstration, this sized die allowed for easier handling and simpler packaging to be developed in order to evaluate individual liquid microlens performance. In addition, having a significant number of microlens cavities on single die helped to ensure there would be some testable liquid lenses in case of yield issues due to microfabrication, liquid filling or final packaging.

To form the liquid microlenses, the test chip was lowered into a small beaker containing the conducting liquid with a thin film of oil on top. Through self-assembly, oil remained in the hydrophobic tapered cavities, surrounded by the conducting liquid [27]. While submerged, a 750-µm thick, ITO coated fused silica cap, with a 1-mm wide, 0.5-mm thick aluminum frame bonded to it was lowered over the test chip, encapsulating the liquid microlenses. Prior to lowering the fused silica cap, epoxy (2216 from 3M) was beaded around the open face of the aluminum frame and allowed to set for 2 hr. Once the cap was in place, the test chip was removed from the beaker and the epoxy seal was allowed to fully cure over a 24 hr period. The sealed chip was wire bonded in a 40-pin DIP, which had a through-hole drilled in the socket region. Finally, the packaged test chip was inserted in a zero-insertion-

Optics EXPRESS

force board mounted connector for optical characterization. Figure 4 shows a fully packaged microlens test chip. The liquid microlenses were formed with dodecane (dyed with Sudan Red, for clarity) surrounded by deionized water. This combination of liquids results in a difference in refractive index of Δn = 0.09. It is noted that the dye was not used in the oil phase for any of the optical characterization studies.

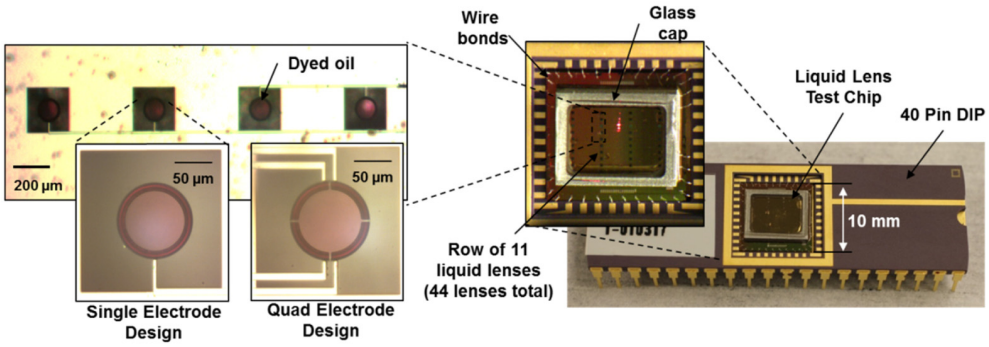

Fig. 4. Liquid filled microlens test chip wire bonded in a 40-pin DIP (right). Test chip contains 44 microlenses. Top down microscope images of the liquid microlenses with an outside diameter of D_o = 110 µm, clear aperture of D_{ca} = 82 µm, and a 45° taper, 12 µm deep, after self-assembly (left). Oil phase: dodecane (w/red dye for clarity), water phase: deionized water.

3. Optical characterization

Because the clear apertures of the liquid microlenses are as small as 32 µm, using a wavefront sensor to measure the focal length would require an optical system that would be large and complex. Instead, we developed a novel approach based on beam magnification. In this approach, the effective focal length is determined by magnifying the beam passing through the liquid microlens and measuring this magnification. Although the eventual operating wavelength is planned to be in the near-infrared, initial characterization was done using a HeNe laser with a wavelength of λ = 633 nm. As illustrated in Fig. 5, the laser beam was first interferometrically collimated with a plane located 75 mm away from a plano-convex lens (f = 75 mm) which focused the beam to a ~16 µm Gaussian diameter spot at focus where the center of the liquid microlens was positioned. The beam then transmits through the liquid microlens and is effectively collimated by a second plano-convex lens (f = 50 mm) before propagating 50 mm to a beam profiling camera (Beamage-4M, Gentec). Different focal lengths of the liquid microlens will result in different beam sizes on the beam profiling camera. Based on the anticipated focal lengths and the optical system, the beam diameters should range from 1 to 10 mm on the profiling camera.

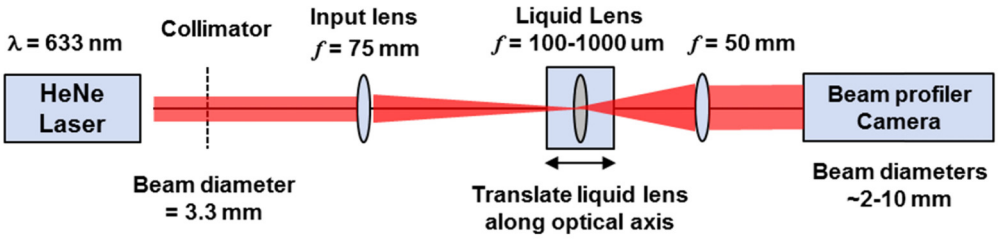

Fig. 5. Illustration of the optical test-setup used for liquid microlens characterization.

In principle, if the liquid microlens is aligned precisely in the optical diagnostic system, then its focal length could be determined directly from the measured beam size. However, this is difficult in practice. Consequently, the liquid microlens is also translated along the optical axis of the optical system and the beam size recorded at multiple locations. These additional

Optics EXPRESS

measurements provide sufficient data to relax the alignment tolerance of liquid microlens, while improving the precision of the focal length measurement. In this work, the liquid microlens is translated a few hundred microns along the optical axis in steps of 20 μm, using a linear motorized stage, with the beam diameter and z-position being recorded at each step. These measurements are fit to an analytical expression for the beam magnification, Eq. (2), derived using standard Gaussian beam propagation [33] through the optical system including the liquid lens with only the focal length and position of the liquid lens used as fitting parameters:

$$\frac{D_{ll}}{D_i} = \left[\left(\frac{f_2}{f_1} \right)^2 \left(1 + \frac{z}{f_{ll}} \right)^2 + \left(\frac{\lambda}{\pi D_i^2} \right)^2 \left(\frac{f_1 f_2}{f_{ll}} \right)^2 \right]^{\frac{1}{2}} \tag{2}$$

where D_{ll} is the measured beam diameter, D_i is the collimated input beam diameter, f_1 = 75 mm, f_2 = 50 mm, z is the axial displacement from the nominal position of the liquid microlens, f_{ll} is the unknown focal length of the liquid lens, and λ is the wavelength (633 nm).

To validate the measurement method a microlens array (MLA-S100-f4, RPC Photonics) with a known focal length was used. The microlens array had a lens size of 100 μm and a nominal focal length of 400 μm. Using the method described, a focal length of f = 360 μm was measured. This was within 10% of the manufacturer's advertised value.

3.1 Liquid microlens focus vs. voltage measurements

Based on the simulation results discussed in Section 2.1, focal measurements for the liquid microlenses were first recorded at 17 V. This voltage should be sufficient to change the interface curvature to convex and allow for the beam profile measurements to be sensitive enough to reduce error. Figure 6 shows an example focal length as a function of voltage for liquid microlenses of different sizes. The voltage is being applied as an AC square wave at 250 Hz. The liquid microlenses were filled with dodecane, n_o = 1.421, and deionized water, n_w = 1.33, resulting in a difference between refractive indexes of Δn = 0.09. The data represents the average focal length of three different liquid microlenses (single electrode design) from the same test chip, tested three times each. The error bars are the standard deviation from the data set. The largest spread in the data occurs for the lower voltages when the liquid interface has the least curvature and longest focal lengths. This is consistent with the sensitivity of the measurement system where small variations in the curvature near the transition state will give rise to large variations in focal length.

Included with the measured data are the predicted focal lengths calculated using the lens maker equation for a thin plano-convex lens and the radius of curvature values of the liquid

Optics EXPRESS

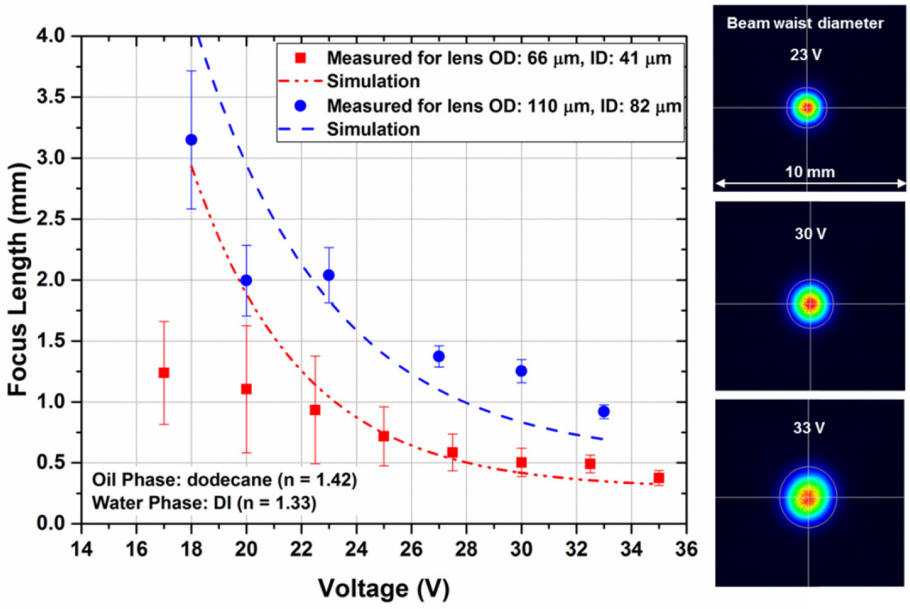

Fig. 6. Measured and predicted focal length vs. voltage for different sized liquid filled with deionized water and dodecane oil (Δn = 0.09). Several images of the beam waist diameters captured from the beam profile camera for different voltages for the liquid microlens with an outside diameter of D_o = 110 µm, clear aperture of D_{ca} = 82 µm, and a 45° taper, 12 µm deep are also included.

interface as a function of voltage extracted from the numerical simulation results. The measured and predicted focal lengths show good agreement, especially at higher voltages when the contact angle changes are large per increases in voltage and the system is less sensitive to small variations to contact angle and the liquid microlens radius of curvature.

The discrepancies between the measured and predicted focal lengths at the low voltages could imply the starting oil-water interface shape is different than what the numerical simulations are assuming. It is assumed the interface is initially concaved and has Young's angle, $\theta° = 23°$. During the self-assemble filling process, a greater volume of oil could be in the cavity, resulting in a larger initial contact angle and a less concave interface shape. The interface could even be convex if a significant amount of oil was dosed. This would affect the initial focal length values, but then they would converge rapidly to the values measured for the higher voltages since changes in the radius of curvature as a function of voltage are not large.

Determining the shape of the oil-water interface inside these liquid microlenses has proven challenging, especially since both liquids are highly transparent. Several optical methods, including 3D microscopy and interferometry have been attempted but have been unable to observe the interface with enough detail. However, the liquid microlenses are operating as a focusing optic and can be repeatedly actuated to different voltages. In addition, the results show that for a liquid microlens formed with dodecane and deionized water (Δn = 0.09) with an outside diameter of D_o = 66 µm, clear aperture of D_{ca} = 41 µm, and a 45° taper, 12 µm deep, a focal range from f = 1 mm to 300 µm was achieved, meeting a design goal and making this lens configuration viable for optogenetics.

The parameters that influence focal length and the liquid interface curvature are: 1) lens size, 2) liquids used to make up the lens (index of refraction difference), and 3) voltage

Optics EXPRESS

through the electrowetting effect. For the results presented in Fig. 6, the lens size is varied, while the liquids were constant. In Fig. 7 the oil phases used to form the liquid lenses were changed and lens size was constant. The focal length vs. voltage was measured for liquid microlenses formed with dodecane and deionized water (Δn = 0.09) and liquid microlenses formed with silicone oil, DC-704 and deionized water (Δn = 0.23) for geometry with an outside diameter of D_o = 110 µm, clear aperture of D_{ca} = 82 µm, and a 45° taper, 12 µm deep. The surface tension for a deionized water/dodecane interface and a deionized water/DC-704 interface are nearly the same, $\gamma_{wo} \cong 45$ mN/m, thus similar voltages will be required. The results show a much shorter focal range for the higher index oil, as expected, from f = 0.5 mm to 0.25 mm, compared to f = 3.2 mm to 0.9 mm for the much lower index oil. Figure 7 also illustrates one of the advantages of liquid lenses. By simply changing the liquids, new lensing performance can be achieved for the same geometry.

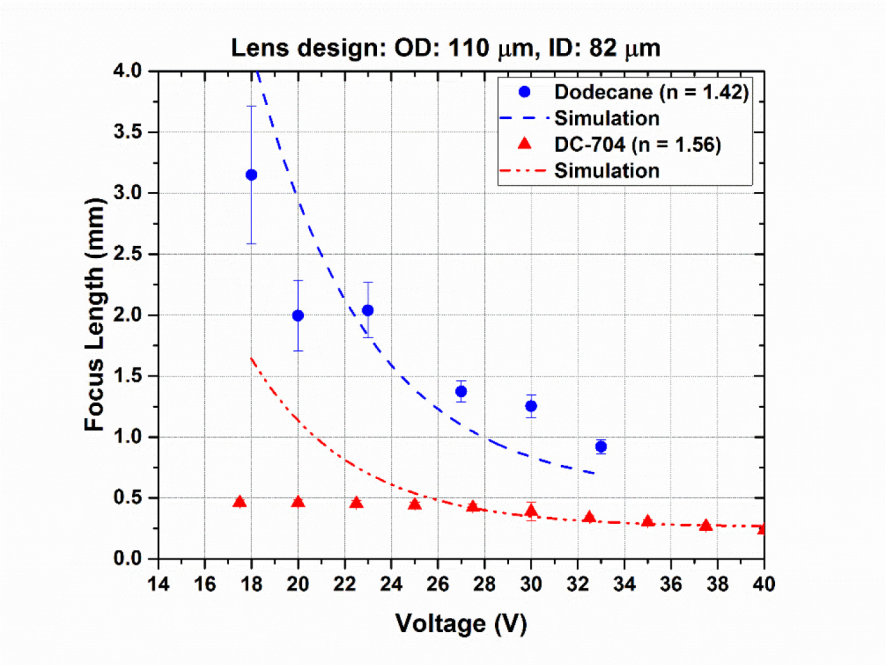

Fig. 7. Measured and predicted focal length vs. voltage for different liquid microlenses filled with different oil phases but constant lens cavity geometry. One set of liquid lenses were filled with deionized water and dodecane oil (Δn = 0.09). The other set of liquid lenses were filled with deionized water and silicone oil, DC-704 (Δn = 0.23). The liquid microlens had a geometry with an outside diameter of D_o = 110 µm, clear aperture of D_{ca} = 82 µm, and a 45° taper, 12 µm deep.

3.2 Beam steering measurements

To steer the beam and simultaneously focus, requires the curvature of the liquid lens to maintain a spherical profile while being tilted. The design of the quadrupole electrode arrangement around the conical taper allows for multiple contact angles to form along the three-phase contact line depending on the voltage being applied to each electrode. Since the dielectric film thickness is the same over each electrode in this design, meaning the capacitance is the same, the amount of contact angle change, i.e. electrowetting force at the three-phase contact line, will be a function of voltage only. The higher the voltage, the larger the electrowetting force being applied and greater the contact angle change. Between the combination of cone angle of the microlens cavity, and different voltages applied to each of the four electrodes, the liquid interface will tilt within the cavity since the three-phase contact

Optics EXPRESS

line will displace to different locations along the sidewall. Figure 8 shows the results of a 2D two-phase numerical simulation (details discussed in Section 2.1) where different voltages were applied to the taper sidewalls for a liquid microlens design with an outside diameter of D_o = 110 µm, clear aperture of D_{ca} = 80 µm, 45° taper, 15 µm deep. As the figure shows, the amount of tilt and curvature of the liquid interface will depend on the difference in electrowetting force at each electrode. Based on the oil-water interface curvature, the amount of beam steering was estimated to be $\delta = \pm 0.8°$ for conditions in Fig. 8(b) and $\delta = \pm 1.1°$ for conditions in Fig. 8(c) for Δn = 0.09 and $\delta = \pm 1.8°$ for conditions in Fig. 8(b) and $\delta = \pm 2.5°$ for conditions in Fig. 8(c) for Δn = 0.23. These estimated steering angles are below the desired goal, but can still provide 10's of microns of beam displacement in order to target a neuron cell body.

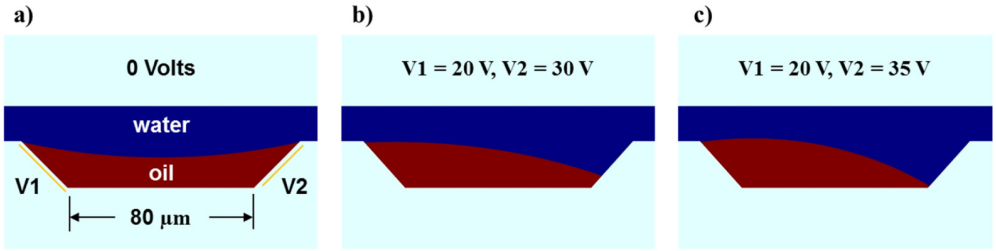

Fig. 8. 2D laminar two-phase numerical simulation results for different sidewall voltages, *V1* and *V2* for a liquid microlens geometry with an outside diameter of D_o = 110 µm, clear aperture of D_{ca} = 80 µm, and a 45° taper, 15 µm deep. The liquid properties used in the simulations were deionized water and dodecane oil. The dielectric thicknesses used for the electrowetting contact angle calculations were t_{oxide} = 500 nm, and t_{CYTOP} = 85 nm.

To measure the amount of beam steering, the same optical setup was used as for the focus measurements. When different voltages are applied to the quadrupole electrode arrangement on liquid microlens, the centroid position recorded on the beam profiling camera shifts. Knowing the distance from the liquid microlens to the plano-convex lens located just before the beam profiling camera, the steering angle can be determined from the change in centroid position compared to the zero voltage centroid position.

Figure 9 plots the change in centroid position of the beam waist diameter from the zero voltage state for four different voltage states, for a liquid microlens formed with dodecane and deionized water (Δn = 0.09) having a geometry with an outside diameter of D_o = 110 µm, clear aperture of D_{ca} = 82 µm, and a 45° taper, 12 µm deep. The inserts in Fig. 9 indicate which electrode pair is at a larger potential. The shaded electrode pair in this case is receiving 30 Vac, while the other pair of electrodes is receiving 20 Vac. Based on the displacement of the centroid of the beam waist diameter and the distance to the plano-convex lens (d = 50 mm), the steering angle was found to be, $\delta = \pm 0.4°$. This steering angle can be increased or decreased based on the voltage difference, the index of refraction, and lens size.

When the voltage difference between the electrode pairs was increased a larger beam displacement was observed as shown in Fig. 10(a). However, there was more asymmetry of the centroid position for larger voltage differences compared to the results in Fig. 9. The asymmetry created a range in steering angle from δ = 0.5° to 0.9°. Even with the increased asymmetry of the centroid position about the zero voltage state, the shape of the beam waist was not affected; a circular shape was still observed on the camera which indicates a spherical shape of the liquid interface at least for the region of the microlens the laser beam is passing through.

Optics EXPRESS

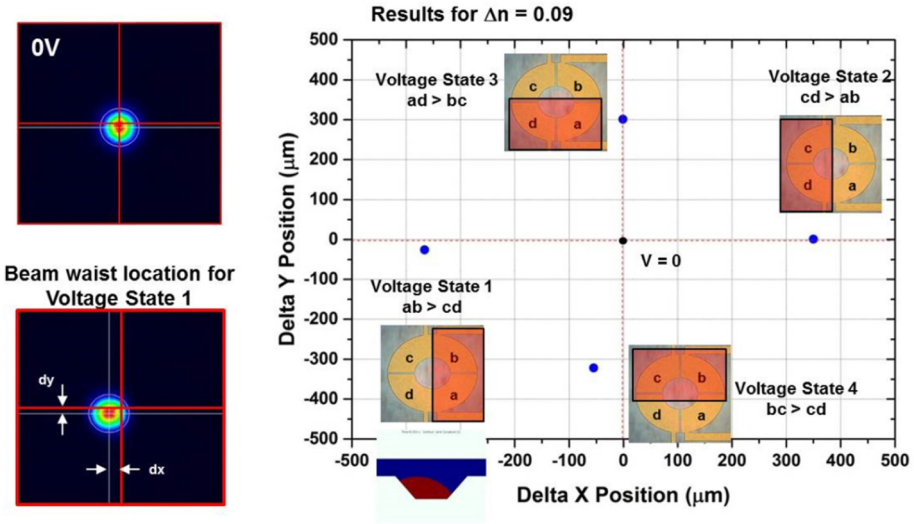

Fig. 9. Changes in beam waist diameter centroid position for four different voltage states. The shaded electrodes are receiving 30 Vac and the other electrode pair is receiving 20 Vac. The liquid microlenses were filled with deionized water and dodecane oil (Δn = 0.09) and had a geometry with an outside diameter of D_o = 110 μm, clear aperture of D_{ca} = 82 μm, and a 45° taper, 12 μm deep.

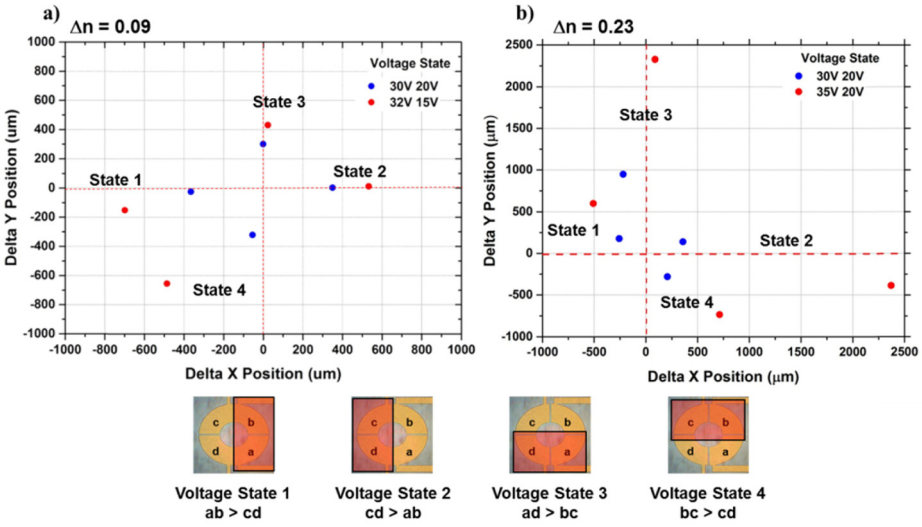

Fig. 10. Comparing beam waist displacement for different voltages and liquid lenses filled with different oils. The shaded electrodes are receiving higher voltage than the other electrode pair. a) The liquid microlenses were filled with deionized water and dodecane oil (Δn = 0.09) and had a geometry with an outside diameter of D_o = 110 μm, clear aperture of D_{ca} = 82 μm, and a 45° taper, 12 μm deep. b) The liquid microlenses were filled with deionized water and silicone oil, DC-704 (Δn = 0.23) and had a geometry with an outside diameter of D_o = 110 μm, clear aperture of D_{ca} = 82 μm, and a 45° taper, 12 μm deep.

Figure 10(b) plots the change in centroid position of the beam waist diameter from the zero voltage state for four different voltage states for a liquid microlens formed with silicone oil, DC-704 and deionized water (Δn = 0.23). As expected, the centroid position of the beam waist displaced more as compared to the liquid microlens of the same size having a Δn = 0.09.

Optics EXPRESS

However there was considerably more asymmetry. Table 1 summarizes the steering results for the liquid microlenses filled with different liquids.

Table 1. Calculated steering angle from measured centroid position.

Voltage State	Steering Angle δ (degrees) Δn = 0.09		Δn = 0.23	
	30V/20V	32V/15V	30V/20V	35V/20V
1	0.42	0.82	0.40	0.90
2	0.40	0.61	0.44	2.75
3	0.35	0.50	1.11	2.67
4	0.37	0.94	0.40	1.17
Avg.	***0.39***	***0.72***	***0.59***	***1.9***

The beam steering asymmetry could be the result of several factors. One is possible variations in the dielectric film thickness, especially that of the hydrophobic film. This would result in a non-uniform capacitance over the electrodes and thus an electrowetting force imbalance for the same voltage. Since the hydrophobic film was applied using a spinning process, an annular thickness variation could exist, especially since the film is being applied over topology. Other coating methods such as a dip coating or spray coating could be employed to help mitigate a film thickness variation.

Another reason for the asymmetric steering behavior could be caused by the pinning of contact line of the liquid interface at the solid substrate [34, 35]. Contact line pinning is possible since the side wall etch does roughen the surface slightly as seen in Fig. 3(d), thus potentially increasing the contact angle hysteresis. In addition, the hydrophobic film is patterned and the resulting transition from hydrophilic-to-hydrophobic can result in the contact line getting pinned. In our previous work [27] we have observed a lag between a change in contact angle and the voltage required to move the interface near the hydrophobic/hydrophilic transition. Increasing the AC frequency has been shown to overcome some contact line pinning issues [34] and will be explored in future efforts.

4. Conclusions

An electrowetting-based micron-scale liquid lens that combines both adjustable focusing and beam steering in a single optical element has been successfully demonstrated. The liquid microlenses were designed to support optogenetic *in vivo* mapping of brain activity by being able to focus light down to a spot size of ~10 μm for single neuron cell resolution. Both adjustable focusing and beam steering were achieved through a novel design of the lens cavity that had a 45° conical taper, etched 12 μm deep into a fused silica substrate, and interdigitated electrodes patterned along the side walls. This design allows for the liquid interface, formed between two immiscible liquids, to uniformly change its radius of curvature along the optical axis when the same voltage is applied to each electrode, or tilt the interface while maintaining a spherical shape when different voltages are applied to each electrode and thereby steer the beam.

To form the conical taper, a grayscale-lithography process was developed which included designing a photolithography mask with sub-resolution annular lines with radially varying line widths. The photomask design created an appropriate tapered profile in photoresist which was then transferred into the fused silica substrate using an optimized RIE process that produced the correct taper profile. Tapered microlens cavities having clear apertures ranging from 32 μm to 82 μm were fabricated.

Liquid microlenses were packaged with a water-oil phase combination of deionized water and dodecane, and other liquid microlenses were packaged with deionized water and silicon oil, DC-704, in order to evaluate the effect the difference of the index of refraction had on focusing and beam steering. Because the clear apertures of the liquid microlenses were as small as 32 μm, we developed a novel approach based on beam magnification to determine the focal length of the liquid microlenses. Tunable focusing ranging from 0.25 to 3 mm and beam steering of ± 1 degree were demonstrated. Asymmetric behavior was observed during

Optics EXPRESS

beam steering measurements, which was attributed to a potential variation in the dielectric film thickness of the hydrophobic film that covers the electrodes and/or contact line pinning.

The measured steering angles were lower than the desired design goal of ± 5°. However, the steering angles achieved were expected, based on the final microlens cavity design fabricated in this phase of the project. One way to increase the steering angle, besides just increasing the refractive index of the oil phase would be to increase the tilt of the interface. This could be achieved through a steeper taper angle, and having a deeper taper cavity. In this work, the depth of the cavity was limited to ~12μm which was a compromise of what we could easily fabricate. Using a hard mask, for the grayscaling is not possible, thus the photoresist most be thick enough to withstand the deep fused silica etching process. Based on the fabrication lessons learned, increasing the cavity depth by 2X is possible.

Funding

National Institute of Health (NIH) (5R01DA029639).

Acknowledgments

The authors would like to thank Mark Townsend for help with developing the grayscale-lithography photomasks and the staff in the Microelectronics Laboratory at Lincoln Laboratory, in particular Dmitri Shapiro and Matthew Cook. Portions of this work were presented at the OSA Biophotonics Congress: Optics in the Life Sciences in 2017, "Adaptive fluidic microoptics for single cell optogenetics." This material is based upon work supported by the MIT under Air Force Contract No. FA8721-05-C-0002 and/or FA8702-15-D-0001. Any opinions, findings, conclusions or recommendations expressed in this material are those of the author(s) and do not necessarily reflect the views of the MIT.